communications sustainability

A Nature Portfolio journal

Article

https://doi.org/10.1038/s44458-026-00100-3

Speeding incurs substantial environmental and economic costs nationwide for negligible travel time savings

Check for updates

Bharat Jayaprakash & William F. Northrop

Speeding is a known contributor to high energy use and emissions in road transport, yet its large-scale impacts remain underexplored. Here, we analyze over 120 million vehicle trajectories from four representative days in 2021 to quantify energy consumption, costs, and emissions from speeding for light-duty internal combustion engine vehicles across the continental United States and Hawaii and for battery electric vehicles in California. Two speed limit interventions on highways and arterial roads are evaluated and extrapolated to the national vehicle fleet. We estimate that adherence to posted speed limits could save more than 6 million gallons of fuel, 18 million US dollars, and 50,000 metric tonnes of carbon dioxide per day, while increasing travel time by only 54 seconds per driving day. On an annual basis, these savings are comparable to removing about 5.5 million conventional passenger vehicles from the road.

Light-duty (LD) vehicles, those under 8500 lbs, account for 14.6% of total energy consumption in the United States[1,2]. In 2023, an average of 376 million gallons of motor gasoline per day[3] was consumed nationwide, equating to 3.19 million metric tons of carbon dioxide (CO_2) emitted. At an average gasoline price of $3.52 per gallon[4], this translates to a daily expenditure of approximately $1.32 billion for internal combustion engine vehicles (ICEVs). Battery electric vehicles (BEVs), accounting for the majority of the U.S. LD fleet's 2.25% plug-in electric vehicle share[5,6], consumed a total of 8.66 million MWh of electricity in 2024[7], resulting in a daily electricity cost of approximately $4.03 million[8]. Assuming a marginal emissions factor of 3.94×10^{-4} metric tons CO_2 (tCO_2) per kWh[9], an estimated daily 9348 tCO_2 was emitted to generate the electricity required for charging BEVs.

The aerodynamic drag force acting on a moving vehicle increases with the square of speed[10], making high-speed driving disproportionately energy-intensive. Fuel economy declines at low average speeds during stop-start operation and again at high speeds as aerodynamic drag dominates, with an optimum between 40 and 55 mph for light-duty vehicles[11]. This range informed 1970s-era highway speed limit regulations[12]. Subsequent increases in posted speed limits on highways from 55 to 70 mph increased ICEV fuel consumption by up to 38%[13], while decreasing limits on urban roadways has had the opposite effect[14]. Driver deviations from posted speed limits have a consistent and quantifiable impact on energy use and emissions: on highways, even a modest 10 mph increase in cruising speed over the limit can raise ICEV fuel consumption and CO_2 emissions by up to 21%[15]. BEVs exhibit similar increases in energy consumption due to speeding and aggressive acceleration, though regenerative braking has a mitigating effect[16].

Although the effects of speed on energy consumption can be quantified, the resulting penalties are not substantial enough to change average driving behavior[17–19]. This conclusion is evidenced by increased vehicle speeds measured on U.S. roadways during the COVID-19 pandemic in 2020 and into at least the first half of 2021[20]. Previous research has neither examined the nationwide energy cost at high spatial resolution nor estimated the impact of slower driving at scale. Without quantitative analysis of representative spatial data, policymakers and fleet managers cannot target interventions that maximize fleet-wide benefits.

Here, we combine real driving trajectories with energy consumption models to estimate the overall impact of speeding on energy use and CO_2 emissions for the U.S. LD vehicle fleet. Using a unique, large-scale spatial telematics dataset of 120 million trips over four days, one from each season in 2021, we (1) quantify and visualize speeding prevalence across regions of the U.S., vehicle classes, and seasons; and (2) estimate nationwide energy, cost, and emissions reductions achievable through adherence to posted speed limits. To enable this, we apply two interventions on the trajectories to reduce vehicle speeds on highways and arterial roads, compare energy consumption using physics-based models, and extrapolate the resulting impacts to the entire U.S. fleet. The analysis covers ICEVs across the continental U.S. and Hawaii, while BEVs are examined in California, the only

Department of Mechanical Engineering, University of Minnesota Twin Cities, Minneapolis, MN, USA. e-mail: jayap015@umn.edu; wnorthro@umn.edu

state with a sufficiently large BEV share (2.7%). We therefore report ICEV and BEV results within their respective geographic domains.

Results

Throughout this study, we perform analysis on the observed vehicle fleet and extrapolate the results to a larger vehicle population. All analyses are limited to LDVs and correspond to the same four 24-h periods represented in the telematics dataset. The observed ICEV fleet refers to the set of ICEV trips from the continental U.S. and Hawaii captured in our dataset. All trip-level behavioral and energy-related estimates are computed within this observed fleet. The extrapolated ICEV fleet refers to national projections obtained by scaling aggregated daily savings using reported state-level total vehicle miles travelled (VMT) statistics. Similarly, the observed BEV fleet consists of BEV trips captured in our dataset and observed in California only. The extrapolated BEV fleet refers to California-wide fleet-level estimates derived by scaling observed BEV results using state-level VMT data.

State of speeding in the U.S

Speeding, defined as when a vehicle exceeds the locally posted speed limit, is highly prevalent in the U.S. In this study, we define a speeding event as any instance where the vehicle's instantaneous speed exceeds the locally posted speed limit by any positive margin (>0 mph) for at least one discrete timestamp within the trajectory, restricted in this analysis to segments on highways and arterial roads with speed limits greater than or equal to 45 mph. We examine three speeding metrics in this work: (1) speeding prevalence, defined as the percentage of trips containing at least one speeding event; (2) maximum speed excess, defined for each trip as the maximum positive deviation (in mph) between the vehicle speed and the posted speed limit observed at any point during that trip, capturing high-risk speeding behavior; and (3) speeding time share, defined as the percentage of trip time spent speeding for those trips identified as having at least one speeding event. Rationale for these metrics is provided in "Methods." We choose a spatial resolution of 3-character geohashes to maintain consistency when reporting these metrics and subsequent results.

Within the observed ICEV fleet, 43.2% of trips have at least one speeding event. On average, these trips exhibited a mean maximum speed excess of 11.2 mph and spent 11.75% of their duration above the speed limit. This estimation is conservative because the analysis considers only speeding on highways and arterial roadways. By state, the percentage of ICEV trips speeding is notably higher in the southeast states, including Florida (54.61%), Georgia (56.44%), North Carolina (62.11%), and certain regions of Alabama (48.09%) and Virginia (53.84%) (Fig. 1a). In contrast, northwestern states like Montana (20.45%), Wyoming (26.32%), Idaho (26.33%), North Dakota (26.73%), and South Dakota (21.83%), as well as much of Nevada (29.99%), exhibit relatively lower speeding prevalence, which may be explained by higher posted limits in those states. Since speeding prevalence in Fig. 1a is calculated as a percentage of all observed trips, the illustrated regional variation is a product of both local driver behavior and the density of the arterial roadway network that provides the opportunity for such behavior to occur. To evaluate the potential confounding influence of regional roadway infrastructure, we conducted a comprehensive sensitivity analysis, where we contrasted our primary definition of speeding prevalence with a formulation for speeding propensity, defined as the ratio of speeding trips to eligible trips containing at least one arterial or highway segment. As detailed in the Supplementary Note 1 and Supplementary Fig. 1, we found a high Pearson correlation of $r = 0.91$ between the original speeding prevalence and the fraction of eligible trips within each geohash, whereas a significantly lower correlation of $r = 0.41$ was observed between the original prevalence and the refined speeding propensity. These results demonstrate that the spatial heterogeneity observed in Fig. 1a is highly influenced by the functional composition of the regional roadway network rather than driver behavior in isolation.

The spatial variation of the mean maximum speed excess across geohashes (Fig. 1b) is lower than that of speeding prevalence. States with high speeding prevalence, namely, Florida (11.61 mph), Georgia (11.56 mph), North Carolina (10.72 mph), and Virginia (11.52 mph), do not necessarily exhibit the highest mean speed excess. Northwestern states, such as Montana (9.77 mph), Wyoming (9.30 mph), Idaho (8.75 mph), and South Dakota (10.12 mph) show both low speeding prevalence and speed excess. Notably, parts of Nevada display elevated speeding prevalence despite posted limits of 80 mph, with one region (near the northeastern border of the state) observing a mean maximum speed excess of 25.42 mph, raising the state's mean to 12.84 mph.

Small sport utility vehicles (SUVs) and small pick-up trucks exhibit lower values of mean maximum speed excess, generally under 11 mph (Fig. 1d). Standard pick-up trucks and large SUVs have slightly higher values. More agile vehicles, like subcompact cars, midsize cars, and two-seaters, exhibit greater magnitudes of speeding. Two-seaters exhibit a mean speed excess of 15.41 mph, with one standard deviation (σ) above the mean reaching 27.08 mph.

We find that speeding prevalence remains statistically consistent across seasons, with trip-weighted mean values between 43 and 45% (Fig. 1e). The upper quartile is lowest in winter (January), increases through spring (April) and summer (August), and then decreases again in the fall (October). The trip-time-weighted average speeding time share, as shown in Fig. 1f, ranges from 18.5% (in August) to 19% (in January). The distribution is narrowest in January, with a σ of 2.83 percentage points and widest in October, with a σ of 3.08 percentage points. The weights used for calculating the mean speeding time share are the total aggregated trip durations of speeding trips in each geohash, which is the denominator used to calculate the metric. Because Fig. 1f summarizes geohash-level average behavior, it does not reflect the full distribution of per-trip speeding. Accordingly, Supplementary Fig. 3a, b present trip-level histograms of both the percentage of time spent speeding and the maximum speed excess, respectively, which characterize typical and extreme speeding behavior across individual trips and reveal strong right-skewness not visible in spatial averages. For ICEV trips involving speeding, the median speeding time share is approximately 13–14%, with a maximum speed excess of approximately 10–11 mph.

Since the BEVs in the dataset belong only to subcompact cars and small station wagons, we restrict the California ICEV analysis to the same vehicle classes to ensure comparability. Within these classes, BEV trips exhibit lower speeding prevalence than ICEV trips. The percentage of ICEV and BEV trips speeding in California, averaged by geohash-level trip count, is 43.50% and 37.45%, respectively (Fig. 2a). The choropleth maps of ICEV trips in Fig. 2b, d are also generated using data from the same two vehicle classes. Metropolitan regions like San Francisco and Los Angeles exhibit BEV speeding behavior that aligns closely with the statewide mean. A larger share of ICEV trips is observed to speed in the northeastern region of California relative to BEV trips (Fig. 2b). The mean maximum speed excess is 11.01 mph for BEV trips and 14.73 mph for ICEV trips.

Seasonally, spring (April) had the lowest speeding prevalence among BEV trips (31.51%), while summer (August) showed the highest (40.56%), as well as the most extreme speeding geohash (67.57% in "9qj") (Fig. 2e, f). The lower speeding prevalence observed in April may be partially influenced by shorter trip lengths during this period (5.75 miles), which limited opportunities for sustained high-speed driving, compared to 6.04 miles in January, 7.11 miles in August, and 7.15 miles in October. Speeding BEV drivers tend to spend an average of 19.8% of total trip time above speed limits in January, which decreases to 17.4%, 17.1%, and 16.4% in April, August, and October, respectively. Comparison shows that subcompact BEV trips exhibit substantially lower speeding prevalence and a smaller mean maximum speed excess than ICEV trips of the same class (32.57% vs. 43.57%; 8.87 mph vs. 14.82 mph). This gap narrows for small station wagon trips, where the speeding prevalence (37.54% vs. 40.78%) and mean maximum speed excess (11.05 mph vs. 11.37 mph) of BEV trips are much more comparable to those of ICEV trips. A detailed summary of these speeding characteristics across both vehicle classes and powertrain types for trips in California on each of the four days is provided in Table 1.

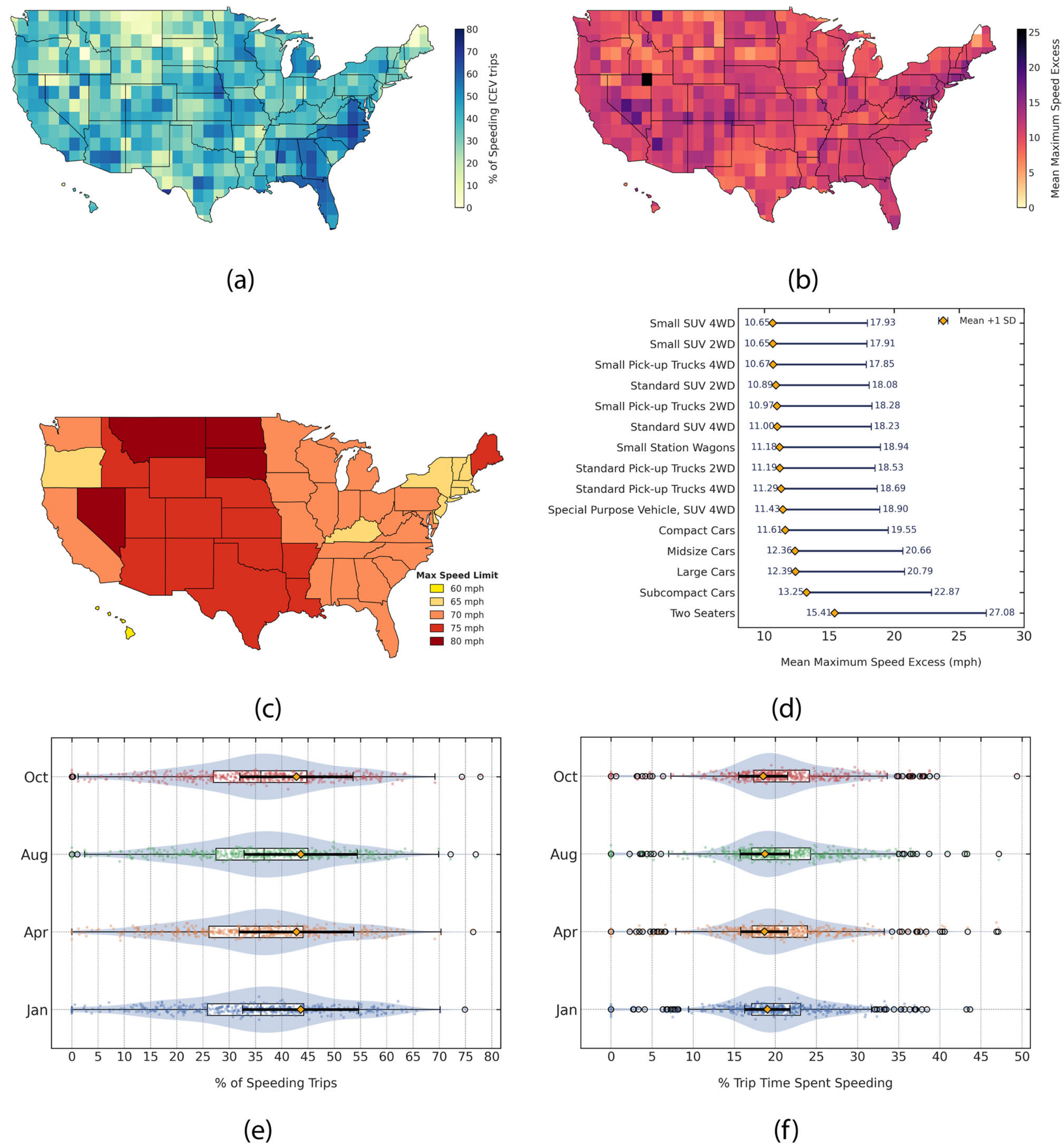

Fig. 1 | Summary of speeding characteristics for the observed ICEV fleet. a Shows the speeding prevalence among ICEV trips within each geohash of the continental U.S. and Hawaii. **b** Illustrates the mean maximum speed excess (in mph) within each geohash, defined as the average across trips of the maximum positive difference between vehicle speed and the corresponding posted speed limit. These are generated using data from all 4 days in the dataset. **c** Shows the state-wise maximum reported speed limit (in mph). Note that the distance between the continental U.S. and Hawaii is not depicted to scale in (**a**–**c**). **d** Shows the maximum speed excess for each of the available ICEV classes. **e** Is a raincloud plot that shows how the percentage of speeding ICEV trips in the continental US and Hawaii varies across the 4 days, each representing the 4 meteorological seasons. **f** Is a similar raincloud plot for the percentage of each trip driven above the speed limit for all speeding trips in the continental U.S. and Hawaii. The raincloud plots in (**e**, **f**) consist of three layers: (1) the violin plot (blue, mirror-symmetric kernel-density envelope) shows the full, unweighted distribution of the geohash-level metric (2) the boxplot (white-filled rectangle with whiskers) gives the median (black bar), the inter-quartile range (IQR, box edges are the 25th and 75th percentiles) and whiskers extending to 1.5 × IQR, and (3) the orange diamond with a horizontal whisker which marks the weighted mean and +1 standard deviation of the same metric, so heavily traveled geohashes have proportionally greater influence on this summary point than on the violin and box plots. Trip count and total aggregated trip time across speeding trips are used as weights to calculate the mean values in (**e**, **f**), respectively. 4WD four-wheel drive, 2WD two-wheel drive, ICEV internal combustion engine vehicle, mph miles per hour.

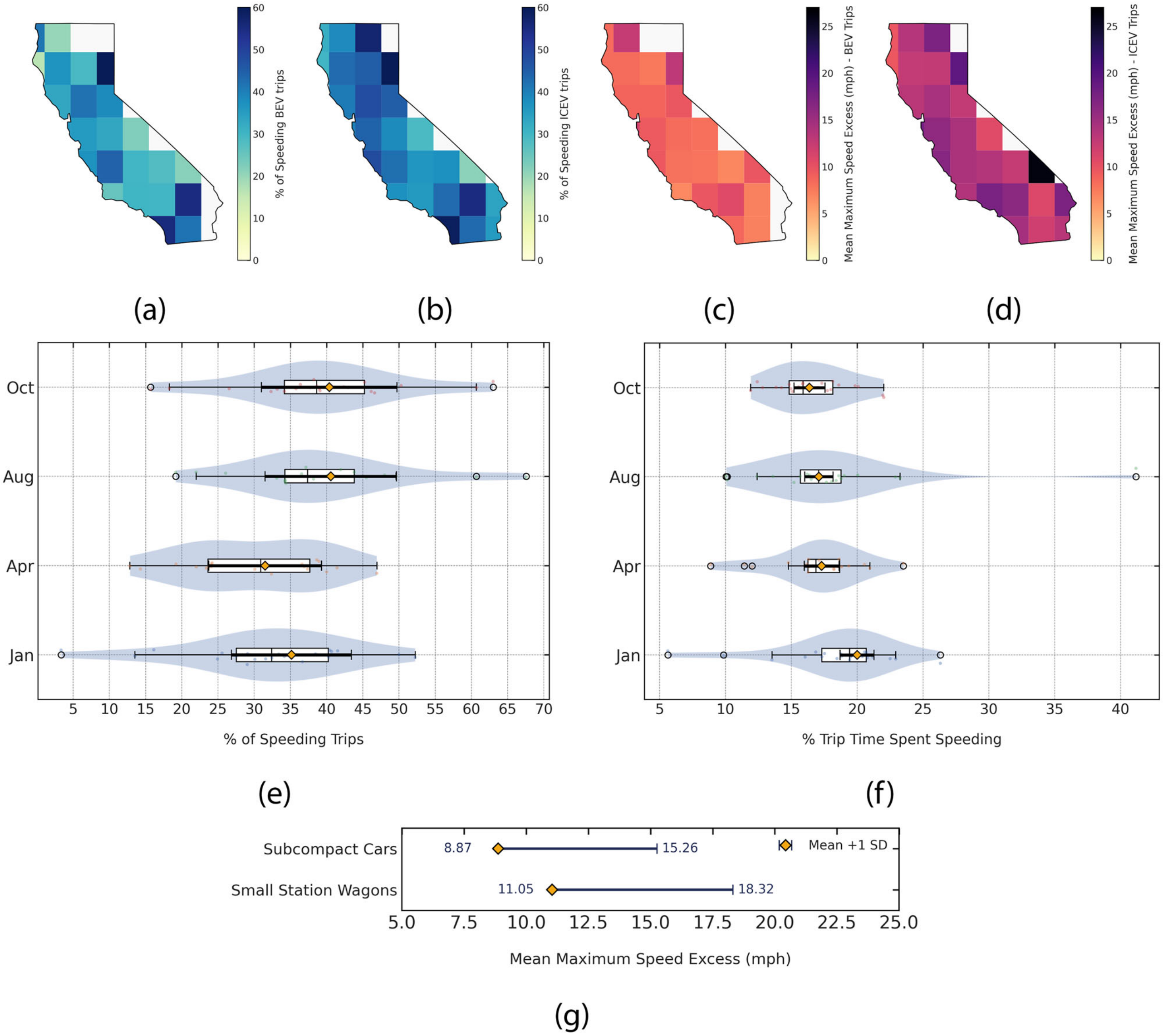

Fig. 2 | Summary of speeding characteristics for the observed BEV fleet. a Shows the speeding prevalence among BEV trips within each geohash in California. The corresponding map for the ICEV trips, using identical legend limits, is shown in (**b**). Geohash cells with fewer than 20 trips (corresponding to the lowest decile of BEV sampling) are shown in white to indicate insufficient data and are excluded from the color scale. Similarly, **c**, **d** illustrate the mean maximum speed excess (in mph) within each geohash in the state for the BEV trips and ICEV trips, respectively, for the same date. These maps are generated using data from all 4 days in the dataset. To ensure a consistent comparison, the ICEV data presented in (**b**, **d**) are restricted to the same vehicle classes (subcompact cars and small station wagons) as the BEV fleet. **e** Is a raincloud plot of the share of speeding BEV trips. **f** Shows a raincloud plot for the percentage of each trip driven above the speed limit for all speeding trips in California. **e**, **f** Contain the same three layers as Figs. 1e, f. **g** Shows the distribution of maximum speed excess for each BEV class in the dataset. ICEV internal combustion engine vehicle, BEV battery electric vehicle, mph miles per hour.

Energy savings due to driving interventions

We implemented two progressively restrictive intervention scenarios, modifying speed profiles in the dataset to reflect increasingly disciplined driving behavior. The interventions preserved total driving distance and route, as described in "Methods." Scenario 1 (SC1) enforces strict speed limit compliance on highways and arterial roads, serving as a conservative bound on the potential energy and emissions savings that can be achieved through regulatory adherence. Scenario 2 (SC2) introduces anticipatory coasting to SC1, implementing smoother decelerations. SC2 is motivated by the observation that prolonged high-speed cruising followed by abrupt slowing to match speed limits results in higher fuel consumption compared to gradual deceleration. Together, SC1 and SC2 capture a range of behavior modifications from compliance to proactive energy-efficient driving. Using FASTSim models[21] calibrated for each EPA vehicle class and powertrain type, we calculated energy consumption for both the original and intervention-adjusted drive cycles. Subsequently, we analyze spatial patterns of energy savings, expressed as gallons of fuel saved for ICEVs and kWh saved for BEVs, across the U.S. to assess regional variation in intervention impacts.

The choropleth maps in Fig. 3a, b illustrate spatial variation in average fuel savings per 100 vehicle miles traveled (VMT) under SC1 and SC2, respectively. These maps are intended to highlight broad spatial patterns in fuel savings rather than support fine-grained quantitative comparisons at the level of individual spatial bins. Quantitative estimates of aggregate fuel savings are therefore presented at the national scale in the latter part of this section.

Under SC1, higher average fuel savings are concentrated along urban corridors in California and parts of Nevada and Arizona. In Nevada, these

Table 1 | Comparing speeding statistics for BEVs and ICEVs in California for each of the 4 days in the dataset characterized by the month

Month	Vehicle	Speeding Prevalence (%)	Mean maximum Speed excess (mph)	Distance travelled Per trip (miles)
January	SC ICEV	44.45	15.58	7.47
	SSW ICEV	41.24	11.49	6.86
	SC BEV	33.49	9.00	5.77
	SSW BEV	35.16	11.37	6.05
April	SC ICEV	43.81	14.90	7.29
	SSW ICEV	41.90	11.55	7.16
	SC BEV	31.26	8.67	5.75
	SSW BEV	31.52	10.93	5.75
August	SC ICEV	43.68	14.56	7.53
	SSW ICEV	38.93	11.56	7.35
	SC BEV	33.51	8.81	5.95
	SSW BEV	40.67	11.05	7.13
October	SC ICEV	42.34	14.25	7.45
	SSW ICEV	40.99	10.92	6.83
	SC BEV	32.01	9.05	5.93
	SSW BEV	40.47	10.94	7.17
Average	SC ICEV	43.57	14.82	7.43
	SSW ICEV	40.78	11.37	7.05
	SC BEV	32.57	8.87	5.84
	SSW BEV	37.54	11.05	6.63

Average statistics consider all trips for calculating speeding prevalence and distance per trip, and all speeding trips for calculating the mean maximum speed excess.
SC subcompact cars, *SSW* small station wagons.

regions align with major east-west and north-south travel corridors, including Interstate 80 and U.S. Route 93, as well as additional corridors associated with U.S. Route 95 further south. By contrast, substantially lower savings are observed across Idaho, Wyoming, the Dakotas, Washington, and much of Montana. Across Hawaii, fuel savings are generally low to moderate. When SC2 is applied, fuel savings increase substantially relative to SC1 in regions where speeding is prevalent, in some cases exceeding a twofold increase. By contrast, regions with little or no recorded speeding, such as parts of northern Maine and central South Dakota, exhibit negligible savings under SC2. Overall, SC2 expands the magnitude of fuel savings while maintaining the relative spatial heterogeneity observed under SC1.

Time penalty, defined as the total trip time increase incurred from implementing SC1 and SC2, serves as a critical indicator of the penalty cost to drivers. Because speed adjustments are applied only during speeding events, the resulting time penalties are sparse and are therefore reported as averages over total VMT. Under SC1, higher average time penalties are concentrated in regions characterized by more frequent and sustained speeding behavior, where penalties can reach up to roughly 530 s per 100 VMT, whereas substantially lower penalties are observed across much of the central and northern U.S. When SC2 is applied, these spatial patterns persist but with a larger overall magnitude of time penalties in high-speeding regions. Across the full study area, the VMT mean time penalty is roughly 190 s per 100 VMT under SC1 and increases to 260 s per 100 VMT under SC2. These values include trips with no speeding and thus may underestimate the time penalties experienced by individual trips that have had their speed profiles modified in response to the interventions.

Given the representativeness of our spatial telematics dataset, we extrapolate the fuel savings from the interventions to the extrapolated ICEV fleet (i.e., scaled national-level ICEV projections) using observed state-level VMT to illustrate their potential nationwide impact (Fig. 3e). Specifically, per-mile fuel savings estimated from the dataset are scaled by real-world daily VMT in each state. Across the 4 days considered, SC1 yields estimated fuel savings on the order of 6–7 million gallons per day, corresponding to approximately \$18–24 million in daily fuel cost savings, depending on season. Implementing SC2 further increases these savings to approximately 7–9 million gallons per day, or \$22–30 million per day, reflecting the greater reduction in speeding under the more stringent intervention. When weighted by daily VMT across the 4 days, these estimates correspond to average nationwide savings of approximately 6.7 million gallons of gasoline, \$22 million, and 57,000 tCO_2 per day under SC1, and approximately 8.2 million gallons, \$27 million, and 69,000 tCO_2 per day under SC2. The daily fuel savings across the four representative dates show higher values in the months of August and October compared to January. This trend primarily reflects increased baseline VMT during these periods. We observed a strong Pearson correlation of $r = 0.95$ and $r = 0.97$ between total VMT and fuel savings for SC1 and SC2, respectively. The fluctuations in gasoline prices across months and states are reflected in the dissimilar variation in the energy and cost savings in Fig. 3e. State-level extrapolated fuel and cost savings underlying the national estimates, for each of the four days and their four-day average, are reported in Supplementary Tables 3–7. The method used for the extrapolation and its associated assumptions are detailed in "Methods."

After normalizing fuel savings by total fuel consumption and consumer expenditure (Fig. 3f), relative savings exhibit only modest variation across seasons for both interventions. For SC1, normalized fuel savings remain close to 2.4% across all four representative months, while SC2 consistently yields higher relative savings of approximately 2.9–3.0%. The limited spread in these values indicates that, once differences in baseline fuel consumption are accounted for, the effectiveness of both interventions is largely stable across seasons. Across the four days, the percentage fuel savings show a strong correlation with speeding prevalence in the observed ICEV fleet ($r = 0.99$). More moderate correlations are observed with both the fraction of trip time spent speeding ($r = 0.64$) and the mean maximum speed excess ($r = 0.63$). These correlations describe aggregate seasonal relationships rather than causal effects. The comparatively weaker correlations for the latter two metrics may partly reflect differences in how these quantities are defined, as both are calculated only for speeding trips, whereas the speeding prevalence is computed across all trips (similar to the computation of fuel savings). Taken together, these results indicate that seasonal differences in normalized fuel savings are more strongly correlated with how widespread speeding is across trips than with the duration or severity of speeding within individual trips.

For the observed BEV fleet, the choropleth maps indicate that energy savings under SC1 are spatially concentrated along major urban and inter-urban travel corridors (Fig. 4a). Elevated savings are observed across coastal Southern California and along prominent north-south routes (e.g., I-5 and I-15) which connect major metropolitan regions, and support sustained high-speed travel. Higher savings are also evident in parts of northeastern California near the Nevada border, while more moderate savings extend through the Central Valley and adjacent inland regions. Applying SC2 yields a broadly similar spatial distribution but with consistently higher energy savings across most regions.

The observed BEV fleet mirrors the patterns identified in the observed ICEV fleet, with SC2 consistently yielding greater time penalties than SC1 (Fig. 4c, d). Higher time penalties are concentrated along major urban and inter-urban corridors along the western coast. When averaged across all BEV trips in California, the VMT-weighted time penalty increases from approximately 180 s per 100 VMT under SC1 to 230 s per 100 VMT under SC2, indicating a consistent increase in travel-time cost under the more stringent intervention.

Using real-world state-level BEV electricity consumption data for each of the four days, we calculate the per-mile energy and cost savings associated with the SC1 and SC2 interventions in the observed BEV fleet for the

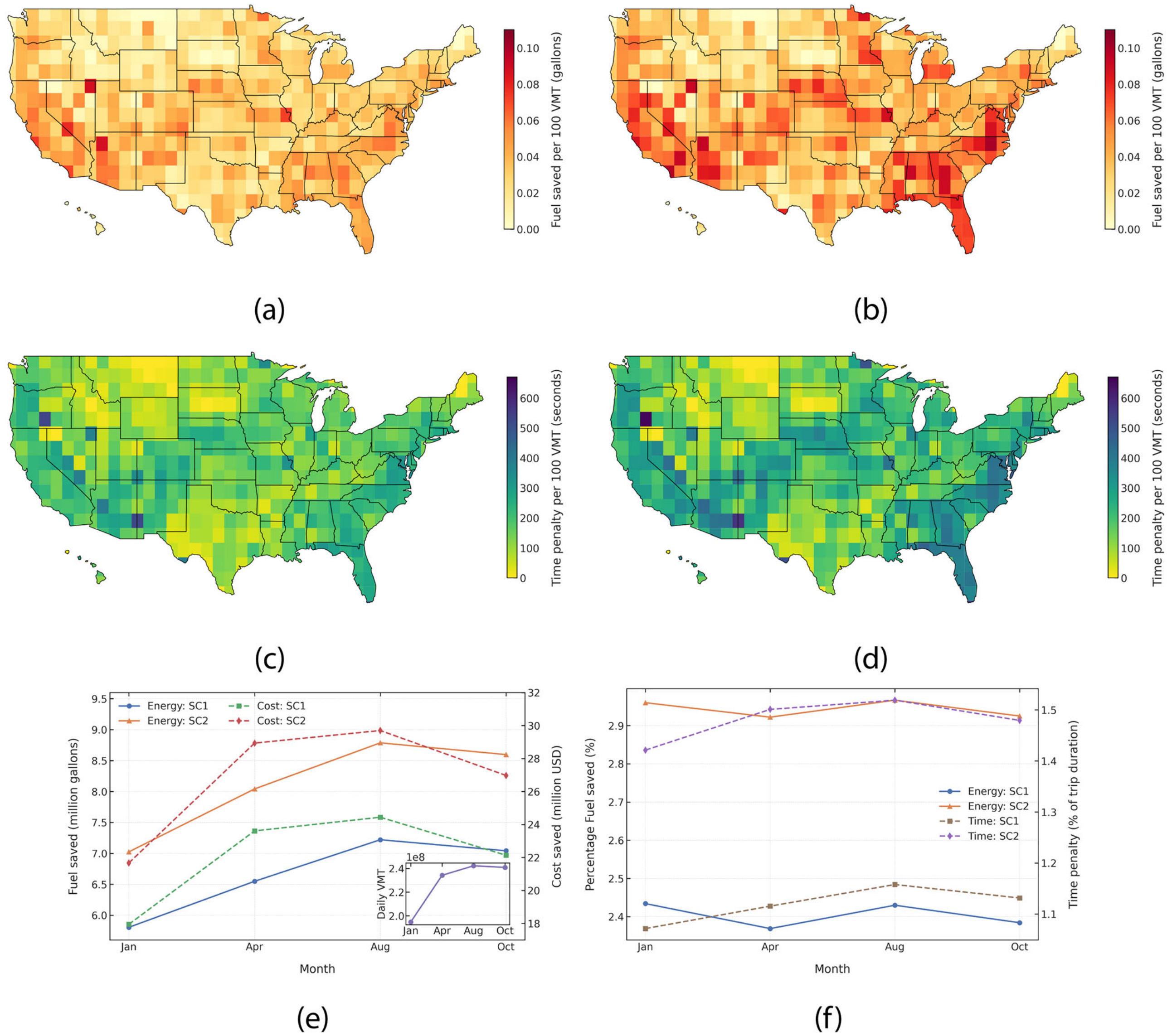

Fig. 3 | Fuel and cost savings due to driving interventions in the observed and extrapolated ICEV fleets. a Shows the spatial variation in average fuel saved per 100 VMT due to SC1 in the observed ICEV fleet using data from all 4 days. **b** Shows the corresponding fuel savings for SC2. **c**, **d** Show the corresponding time penalty in seconds due to SC1 and SC2, respectively. **e** Compares the relative fuel (left y-axis) and cost savings (right y-axis) for SC1 and SC2 in the extrapolated ICEV fleet. The inset plot shows variation in real-world daily VMT by light-duty ICEVs, which varies similarly and may act as a confounding factor. **f** Shows the seasonal variation in fuel and cost savings for the extrapolated ICEV fleet, expressed as a percentage of total fuel consumption and consumer expenditure, and the corresponding variation in time penalty as a percentage of total trip time, for SC1 and SC2, respectively.

extrapolated BEV fleet (i.e., scaled California-wide BEV projections) and illustrate their seasonal variation in Fig. 4e. We then translate the extrapolated energy savings to equivalent emissions estimates. Across the four days considered, SC1 yields energy savings on the order of 160–200 MWh per day, corresponding to approximately 50–90 tCO_2 per day, with associated electricity cost savings of roughly $40,000–45,000 per day, depending on season. Implementing SC2 further increases these benefits, with energy savings of approximately 190–230 MWh per day, emissions reductions of about 60–100 tCO_2 per day, and cost savings reaching around $44,000–52,000 per day. Under both interventions, energy and emissions savings are lower in spring relative to winter, increase during summer, and remain elevated into fall. In contrast, cost savings peak in summer and decline in fall, reflecting seasonal variation in electricity prices. Across all seasons, SC2 consistently yields higher energy, emissions, and cost savings than SC1, while the overall seasonal structure remains similar under both scenarios.

Despite consistent emissions reductions under SC1 and SC2 interventions, the magnitude of charging-related emissions savings depends on the charging schedule and month (Fig. 5). We quantify sensitivity using hourly marginal operating emissions rates (MOER), which represent the additional CO_2 emitted by the grid for each additional unit of electricity demand at a given hour. Emissions savings under the daily and overnight scenarios consistently fall between best-hour and worst-hour bounds. Incorporating weights based on empirically derived BEV charging load profiles[22] leads to modest differences relative to unweighted scenarios, with weighted cases often exhibiting lower emissions savings. Notably, the spread across charging scenarios is substantially smaller in August than in the other months, indicating reduced sensitivity to charging schedule assumptions during that day. Supplementary Table 8 displays the data from Fig. 5 in a tabular format.

In the extrapolated BEV fleet, seasonal variation in total energy savings under SC1 and SC2 broadly tracks variation in total electricity consumption.

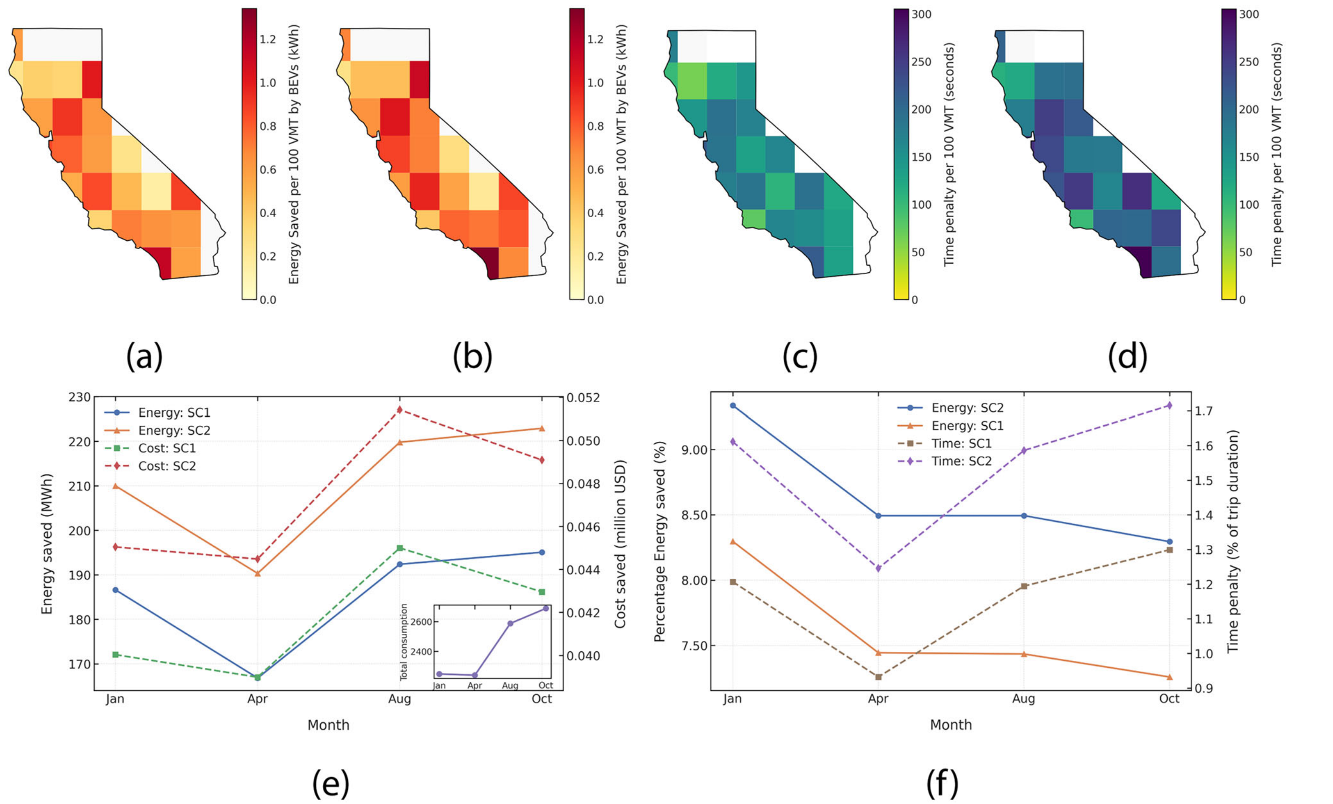

Fig. 4 | Energy and cost savings due to driving interventions in the observed and extrapolated BEV fleets. Energy and cost savings due to driving interventions in the observed and extrapolated BEV fleets. **a** Shows the spatial variation in average energy saved in kWh per 100 VMT due to SC1 in the observed BEV fleet using data from all 4 days. **b** Presents the corresponding energy savings for SC2. Geohash cells with fewer than 20 trips (corresponding to the lowest decile of BEV sampling) are shown in white to indicate insufficient data and are excluded from the color scale. **c**, **d** Show the corresponding time penalty in seconds due to SC1 and SC2, respectively. **e** Compares the relative energy (left y-axis) and cost savings (right y-axis) for SC1 and SC2 in the extrapolated BEV fleet. The inset plot shows variation in total energy consumption (in MWh), which varies similarly to the total energy savings and may act as a confounding factor. **f** Shows the seasonal variation in energy and cost savings for the extrapolated BEV fleet, expressed as a percentage of total energy consumption and consumer expenditure, and the corresponding variation in time penalty as a percentage of total trip time, for SC1 and SC2, respectively.

However, this correlation is weaker than the relationship between fuel savings and daily VMT observed in the extrapolated ICEV fleet, with $r = 0.78$ and $r = 0.84$ for SC1 and SC2, respectively. Contrary to the ICEV case, BEV energy and cost savings percentages are identical (Fig. 4f) because we assume that the electricity price is constant across California. When expressed as a percentage, relative BEV energy savings exhibit a modest but consistent decrease from winter to fall under both interventions, with SC1 savings ranging from approximately 7 to 8.5% and SC2 savings ranging from approximately 8 to 9.5%. For BEVs, the speeding time share and mean maximum speed excess correlate strongly with normalized energy savings under SC1 (r = 0.99 and r = 0.96, respectively), while the percentage of vehicles speeding shows weak correlation with energy savings ($r = -0.35$). This pattern contrasts with ICEV results, where normalized fuel savings are more closely correlated with speeding prevalence than with the other two speeding metrics.

Discussion

Our analysis shows that speed limit adherence can yield meaningful reductions in energy consumption, cost, and emissions across the U.S. for ICEVs at the national scale, and for BEVs within California. While the average percentage reduction in fuel consumption resulting from speed limit adherence in the observed ICEV fleet appears modest, on the order of 2.4–3% depending on season, aggregate impact at the national scale is substantial. The average 6.7 million gallons of fuel saved per day due to SC1 across the extrapolated ICEV fleet translates to approximately 2.4 billion gallons of fuel saved per year, and is equivalent to the annual fuel consumption and associated CO_2 emissions of approximately 5.5 million passenger cars (1.8% of the extrapolated ICEV fleet) or over 220,000 Class 8 trucks in the U.S.[23]. The 195 MWh of energy saved by the extrapolated BEV fleet in a single October day provides enough energy to charge 82 LD BEVs for a whole year[24].

Percentage energy savings are higher in the observed BEV fleet (over 9%) than in the observed ICEV fleet (up to 3%), a pattern that is consistent with known differences in the energy efficiency characteristics of electric and internal combustion powertrains. BEVs maintain high efficiency across a wide range of operating conditions and benefit from regenerative braking, making them more responsive to speed-limiting interventions. In contrast, internal combustion engine efficiency typically increases with power output under typical operating conditions. When vehicle speed is reduced, engine load and efficiency may decrease, partially mitigating the fuel savings achieved from lower aerodynamic drag. The BEV results reported here reflect a limited model sample within the dataset (two BEV production carlines), and these efficiency considerations are presented as plausible mechanisms rather than definitive causal explanations for cross-fleet differences. Accordingly, the differences observed in Figs. 2 and 4 are specific to the BEV configurations analyzed in this study.

The analysis conducted in this study considers only speeding on highways and arterial roadways with speed limits of at least 45 mph, excluding lower-limit roads. This constraint has two implications: (1) true speeding prevalence may be underestimated, and seasonal patterns may be biased because local-road behavior can differ markedly from highway driving; and (2) energy-savings potential may be underestimated because

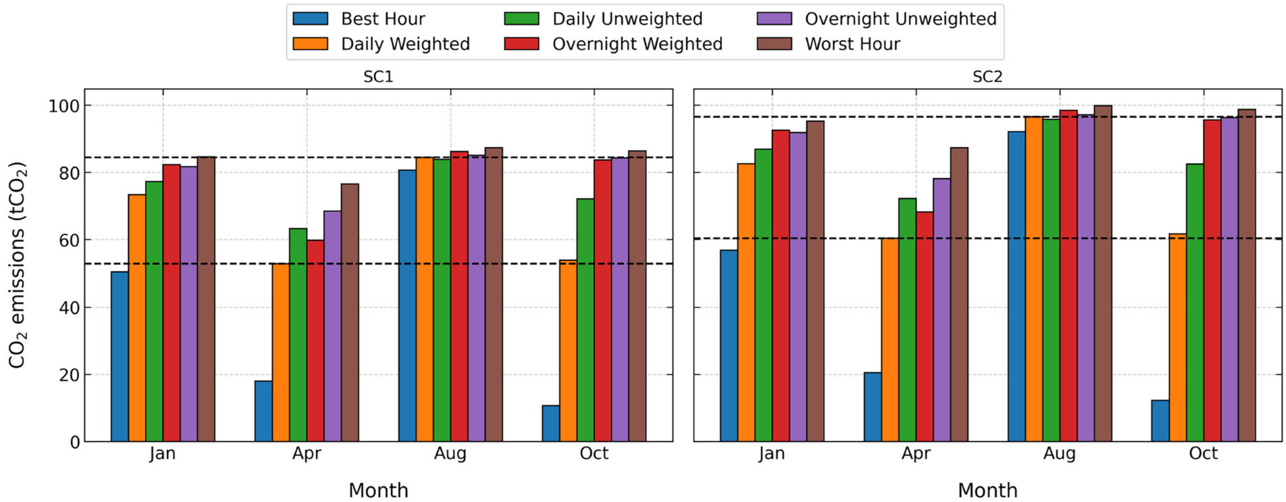

Fig. 5 | Estimated CO_2 emissions savings associated with BEV energy consumption based on charging scenario. For each month, we evaluate five scenarios: distributed charging across the full day, concentrated overnight charging, weighted variants of both, and two idealized bounds corresponding to the lowest and highest hourly MOER values. The weights used in the weighted scenarios (daily weighted and overnight weighted) are the normalized load profiles of residential BEV charging. Overnight hours used to calculate the values for the overnight weighted and overnight unweighted scenarios are chosen to be 10 PM to 6 AM. The best hour scenario considers the lowest hourly MOER value. The worst hour considers the highest hourly MOER value. The dashed horizontal lines represent the upper and lower bounds of the daily weighted scenarios for each of the two interventions.

speeding behavior on lower-speed road segments is not modified or evaluated. Although our analysis limits speed interventions to high-speed corridors, extending them to mixed-road networks and low-speed driving behaviors would likely yield even greater fuel, energy, and cost savings.

Reducing fuel use at scale carries substantial economic implications. Imagining a hypothetical nationwide highway speeding moratorium on a single day in August and the savings due to SC1, the $24 million saved in fuel costs could be largely redirected toward local goods and services. Gelman et al.[25] estimated the marginal propensity to consume (MPC) due to a decrease in gasoline prices to be approximately one, i.e., every dollar a household no longer spends on fuel is matched by almost a dollar increase in other consumption categories. Baumeister et al.[26] also confirm that the savings from lower gasoline consumption largely re-enter the economy as higher consumption and ultimately increase the gross domestic product. Federal and volume-weighted state average motor-fuel tax in the U.S. is 18.40 cents and 32.61 cents per gallon of gasoline[27]. Therefore, the 7.2 million gallons of gasoline saved during the 1-day speeding moratorium would result in a reduction of approximately $3.7 million in motor-fuel tax revenue that states rely on to fund transportation infrastructure. The 7.2 million gallons of gasoline saved also translates to a reduction of approximately 61,000 tCO_2 emissions. At an interim social cost-of-carbon value of $51 per tCO_2 emitted[28], this adds another $3.1 million in avoided climate damages.

The sensitivity analysis of emissions estimation for BEVs illustrated in Fig. 5 shows that the emissions resulting from different charging scenarios can vary based on the MOER values. Since the charging load distributions for the four days are largely similar, the differences in the emissions estimates across the 4 days are largely attributed to the intraday MOER fluctuations. Notably, the estimates for August vary the least, which reflects a flatter intraday MOER profile on that day, likely driven by high solar generation across daylight and evening hours. This is evident from the MOER profile shown in Supplementary Fig. 2a. Under these conditions, reallocating charging demand across hours produces only small changes in marginal emissions, thereby diminishing the influence of specific charging-timing assumptions on emissions. At the same time, our analysis abstracts from several real-world charging contexts, including nonresidential charging (e.g., workplace and public charging), charging using residential rooftop solar panels, and heterogeneous charging strategies across drivers. These factors may alter the emissions intensity of individual charging events, particularly at finer temporal or spatial scales.

Reduction in total trip time is often cited as the rationale for speeding[29]. Our analysis shows that consistently driving at or below the posted speed limit results in a VMT-weighted time penalty of just 190 s per 100 VMT. Using the average daily driving distance of 28.6 miles[30], this corresponds to about 54 s per day, or 6.3 min per week. A 2015 naturalistic driving study from Australia using trip-based averaging found that individual drivers saved an average of 26 s per day and 3 min per week by speeding[31].

For BEVs, the time penalty of 180 s per 100 VMT due to SC1 translates to savings of around 35 s per day and 4.1 min per week. We assume BEVs travel an average of 19.6 miles per day, assuming an annual 7165 VMT[32]. Crucially, beyond an energy cost versus time tradeoff, speeding also carries substantial safety implications. In 2023, 11,775 fatalities in the United States were associated with speeding-related crashes[33]. While eliminating speeding would not prevent all such fatalities, even modest reductions in speeding prevalence could yield meaningful safety benefits. When viewed through this lens, the small time savings associated with speeding offer limited justification relative to its societal costs.

Our results reinforce the notion that the “speeding to save time” paradigm is largely illusory and offers no meaningful benefit to everyday drivers.

Although we focus on the large-scale impacts of the two behavioral interventions, we derive these results from trip-level energy consumption calculations. Our analysis does not account for emergent traffic dynamics that could arise under high penetration rates of the interventions across a fleet. In a real-world deployment, widespread adoption of the SC1 strategy could alter the fundamental relationship between traffic density and flow, potentially leading to scenarios where changes in collective speed profiles influence overall network congestion. Consequently, scaling this to a multi-agent environment poses complex traffic-equilibrium challenges that fall outside the scope of this study. Derivative works should utilize microscopic traffic simulation tools to investigate how fleet-wide adoption impacts system-level throughput and whether individual fuel gains are maintained in high-density scenarios.

Modest behavioral speed-limiting interventions produce consistent, scalable reductions in energy use, costs, and CO_2 emissions. ICEV fuel consumption decreases by between 2.4 and 3% depending on season, which escalates to substantial national-scale impacts. BEV energy use shows analogous material reductions (e.g., 195 MWh saved in 1 October day in the extrapolated BEV fleet, can charge 82 LD BEVs for a year). We find that speeding prevalence is a strong predictor of percentage fuel savings ($r = 0.99$) in the extrapolated ICEV fleet. Seasonal patterns and our highway-only measurement window imply these estimates are behaviorally driven and conservatively represent the full potential across mixed-road networks. The aggregate effects of speeding interventions are economically and societally important: tens of millions of dollars in daily fuel savings across the fleet, millions in avoided environmental impact, and measurable reductions in tax revenue, all without substantial time penalties for individual drivers. These results position driver behavior interventions, including stricter speed limit enforcement and traffic calming measures, as immediately deployable, high-impact strategies for reducing transport energy use, emissions, and cost.

Methods

Data processing

In this study, we use a large-scale connected vehicle dataset obtained from a third-party provider. The original dataset contained time-series vehicle trajectory data collected from millions of vehicles across the United States. The dataset covers four specific 24-h periods in 2021: January 6, April 28, August 11, and October 6. Crucially, all four dates fell on Wednesdays. This consistent mid-week sampling effectively controls for day-of-the-week variability and minimizes travel anomalies typically associated with weekends or holidays. These dates were screened to ensure they did not coincide with major federal holidays or nationwide travel disruptions. While localized weather and regional events were noted on these dates, they were not of a scale or duration expected to fundamentally alter the macro-scale highway speed distributions analyzed in this study.

We then created a derived dataset from the original dataset using a series of transformations: temporal interpolation from 1/3 Hz frequency to 1 Hz frequency, map-matching additional variables using GPS coordinates, deleting the original data points, and imputing missing values at those locations via interpolation. We map-matched road type and speed limit using data obtained from OpenStreetMap (OSM)[34]. Since not all road segments have reported speed limit data in OSM, we imputed missing values using the maximum posted speed limit for the corresponding U.S. state[35]. This conservative imputation ensures that intervention scenarios do not overlook potential speeding behavior in segments where speed limit data is missing. We then map-matched road elevation using data from the 1/3 arc-second resolution digital elevation models released by the United States Geological Survey[36]. To protect driver privacy, GPS coordinates were removed from the derived dataset, ensuring that individual vehicle trajectories cannot be reconstructed. Spatial aggregation was instead performed using 3-character geohashes, which provide a resolution of approximately 1.4° latitude by 1.4° longitude (corresponding to roughly 156 km × 156 km at the equator). There are a total of 503 such geohashes that cover the continental US and another 19 that cover the islands of Hawaii. However, several of these cells encompass unpopulated regions or areas without traversable road networks, particularly across the Hawaiian archipelago, resulting in a subset of geohashes with zero recorded trip trajectories. The attributes for each trajectory in the derived dataset include time, vehicle speed, region code, geohash (3 characters), road elevation, road type, and the speed limit of the road segment. Each trajectory has an associated entry of the make, model, and year of the in-use vehicle. The vehicles represented in the derived dataset are limited to LD passenger vehicles, including SUVs, pick-up trucks, and vans. These vehicles are then grouped based on their electrification level into ICEVs and BEVs. For both of these groups, the vehicles are then classified into a series of vehicle classes. The vehicle classes used in this study are identical to those used by the United States Environmental Protection Agency (US EPA)[37]. Table 2 summarizes the number of vehicles of each vehicle class and powertrain type in the dataset.

Table 2 | Trip counts by powertrain type in the dataset

Vehicle class	Vehicle count	
	ICEVs	BEVs
Subcompact cars	3,072,777	11,207
Special-purpose vehicle SUV 4WD	1,573,032	–
Compact cars	7,076,389	–
Special-purpose vehicle 2WD	651	–
Standard pick-up trucks 4WD	32,641,705	–
Small pick-up trucks 2WD	1,746,721	
Small station wagons	93,557	631,019
Standard SUV 4WD	15,697,123	–
Standard SUV 2WD	10,824,193	–
Small SUV 4WD	12,283,321	–
Small SUV 2WD	25,833,974	–
Standard pick-up trucks 2WD	6,461,518	–
Large cars	3,593,043	–
Midsize cars	9,631,355	–
Small pick-up trucks 4WD	4,805,437	–
Two seaters	366,749	–

Speeding behavior metrics

We use three metrics to characterize speeding behavior: (1) speeding prevalence; (2) maximum speed excess; and (3) speeding time share. We compute speeding prevalence for each geohash by representing the number of trips with at least one speeding event as a percentage of the total number of trips in that geohash. We compute the maximum speed excess and speeding time share for individual trips, assign those trips to their respective geohashes, and then report the average value of each metric across all valid trips within each geohash. The reported mean values of maximum speed excess and speeding time share only consider the trips that contain at least one speeding event. While this may appear at first to bias the averages by excluding non-speeding trips, this conditional summary is designed to answer the question "when drivers exceed the speed limit, how far above it do they go and how much of the trip do they spend doing so?" By conditioning on the presence of speeding, these averages characterize the intensity and persistence of speeding behavior on the subset of trips where it actually occurs. Furthermore, we prioritize a time-based metric for trip share because it represents the total window of risk exposure. While maximum speed excess captures the severity of speeding behavior, speeding time share reflects its persistence. Risk exposure studies[38] support the idea that distance-based risk metrics are inherently sensitive to travel speeds. By using a temporal denominator, we ensure that the speeding share metric consistently measures the amount of time spent engaging in speeding, independent of the magnitude of speed excess. This decoupling is essential for distinguishing between drivers who engage in high-magnitude, short-duration speeding events versus those who exhibit persistent, lower-magnitude speeding.

Energy consumption models

The simplest approach to modeling the energy consumption of vehicles over a given drive cycle involves using the "road load" equation. This equation models the vehicle's longitudinal dynamics to estimate the instantaneous power required at the wheels at each point in the drive cycle, P_{road}. Equation 1 represents one form of the road load equation:

$$P_{\text{road}}(v, v_{\text{w}}, h, t) = \frac{1}{2}\rho_{\text{air}} C_{\text{d}} A (v - v_{\text{w}})^2 v + C_{\text{rr}} mgv + mv\frac{dv}{dt} + mg\frac{dh}{dt} \tag{1}$$

where ρ_{air} is the density of ambient air, C_d is the effective coefficient of drag of the vehicle, A is the effective frontal area, C_{rr} is the coefficient of rolling resistance, m is the mass of the vehicle, g is the acceleration due to gravity, v is the velocity at time t, v_w is the velocity of the head-on wind at time t, and $\frac{dh}{dt}$ is the rate of change of elevation at time t.

In this study, we use FASTSim-based energy consumption models[21], a software package developed by the National Renewable Energy Laboratory. FASTSim uses vehicle parameters (e.g., mass, coefficient of drag, etc.) and the drive cycle (time, speed, and road grade) as inputs to compute energy consumption through a backward-looking approach based on the road load equation. To capture the dynamical differences across vehicle classes, we calibrated one energy consumption model for each class. Figure 6 in illustrates the framework for generating the class-specific energy consumption models. We calibrate each model using two standardized drive cycles and their corresponding dynamometer test results: (1) the EPA Urban Dynamometer Driving Schedule and (2) the Highway Fuel Economy Driving Schedule (HWFET). These tests yield City MPG (miles per gallon) and Highway MPG values, respectively. Their weighted average, known as combined MPG, provides a benchmark for overall fuel efficiency. We obtain these values from publicly available EPA fuel economy data[37]. For each vehicle in the dataset (identified by make, carline, and year), we extract the city, highway, and combined MPG ratings. We then group the vehicles by EPA vehicle class and compute class-level average MPGs, weighted by the number of vehicles in each class. These aggregated values serve as calibration targets for both ICEV and BEV energy consumption models. The computed calibration targets for each vehicle class in our dataset are given in Supplementary Table 1 (ICEVs) and Supplementary Table 2 (BEVs). It is important to note that mileage values for BEVs are represented in units of Miles Per Gallon Gasoline Equivalent (MPGGe). The EPA uses 33.7 kWh of electricity as the equivalent of one gallon of gasoline.

Table 3 shows the set of energy consumption model parameters selected to be calibrated, along with their respective upper and lower bounds. The efficiency maps for the engine and motor are vectors of lengths 12 and 11, respectively, while the other parameters are scalar values. These 1D maps relate efficiency to power output as a percentage of the maximum power, in contrast to conventional 2D efficiency maps, which typically map efficiency to both engine speed and load (e.g., throttle valve angle for engines or torque demand for motors). This simplification reduces the complexity of powertrain modeling while still capturing key efficiency trends. We excluded two key parameters from Table 3: vehicle mass and frontal area. Instead of calibrating these, we treated them as fixed class-specific constants. For each vehicle class, we set the values of mass and frontal area as the weighted average across all vehicles belonging to that class, where the weights reflect each vehicle's share of the total class population.

Table 3 lists the tunable parameters, organized by their associated vehicle subsystem, along with their respective bounds. These configurations specify which category of parameters (as seen in the first column of Table 3) are calibrated based on the vehicle's powertrain type. For ICEVs, the configuration includes vehicle and engine parameters. For BEVs, the configuration includes vehicle, motor, and high-voltage battery parameters. The calibration process begins by defining parameter bounds, followed by iterative optimization using the bounded Nelder–Mead method[39] to minimize the error between simulated and target fuel economy values. We include a penalty function to enforce convexity in the engine efficiency curves and prevent unrealistic non-convex maps. The pseudocode of the calibration algorithm is provided in Algorithm 1 in the Supplementary Information.

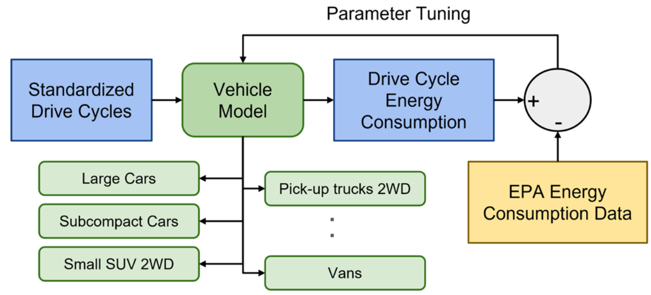

Fig. 6 | Framework for calibrating vehicle models. Parameters of adapted FASTSim vehicle models for each vehicle class were calibrated using standardized EPA drive cycles. For each vehicle model, select parameters were recursively tuned to minimize the error between the averaged EPA energy consumption data and the model-estimated energy consumption.

Table 3 | Energy consumption model parameters selected for calibrating and their respective bound

Category	Parameter	Lower bound	Upper bound
Vehicle	Drag coefficient	0.2	0.8
	Wheel rolling resistance coefficient	0.005	0.015
	Center of gravity height (m)	0.5	1.5
	Wheelbase (m)	2	4
	Drive axle weight fraction	0.4	0.6
Engine	Engine max power (kW)	80	300
	Engine efficiency map	[0.01] × 12	[0.45] × 12
Motor	Motor max power (kW)	60	200
	Motor efficiency map	[0.01] × 11	[0.99] × 11
High-voltage battery	Battery max power (kW)	60	200
	Battery max energy (kWh)	10	150

The bounds for each parameter were chosen based on literature and practical vehicle design constraints.

Driving behavior intervention scenarios

We define two distinct scenarios for driving behavior intervention for this study: (1) speed limit compliance without coasting (Scenario 1), and (2) speed limit compliance with coasting (Scenario 2). Each intervention generates a modified speed profile by scanning the original trajectory and applying targeted adjustments to segments that violate the specific behavioral constraint: exceeding the speed limit. Figure 7 shows a visual comparison of the two scenarios. To aid clarity, we refer to the vehicle following the original (unmodified) speed profile from the dataset as the "source vehicle." A "virtual vehicle" refers to a hypothetical vehicle that follows a modified speed profile under either of the intervention scenarios. Each scenario generates a distinct virtual vehicle profile, which we compare against the source vehicle to assess the impact of the intervention. Both the source and virtual vehicles travel between defined spatial points of interest, which we refer to as "anchor" points. These points correspond to key driving events, such as the start or end of acceleration or deceleration, the point at which the speed decreases to below the speed limit, etc. They are intended to guide the modification process of the speed profiles by acting as bounds between which the modification is applied at a time. To preserve operational validity under real-world traffic conditions, we constrain the virtual vehicle to travel the same distance as the source vehicle between each pair of anchor points. This condition ensures that the modified behavior remains feasible given the context in which the original data were recorded.

When Scenario 1 is applied to a source vehicle's speed profile, the virtual vehicle's speed is capped at the posted speed limit at all times. To enforce the distance constraint within a speeding segment, such as the one between timestep 300 and 450 in Fig. 7a, the virtual vehicle maintains the speed at the limit until it has traveled the same distance as the source vehicle. As a result, the virtual vehicle begins to decelerate slightly later than the

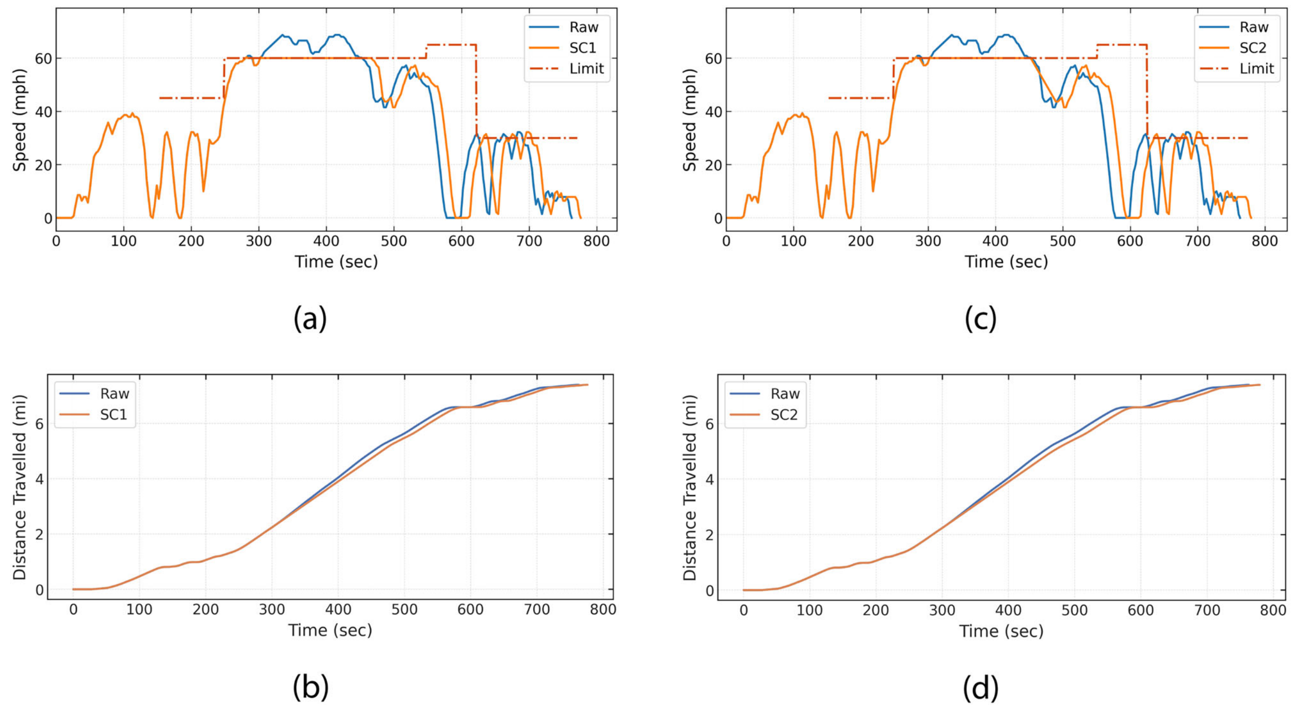

Fig. 7 | Comparison of vehicle speed and distance across Scenario 1 and Scenario 2. a Raw vehicle speed and adjusted speed under Scenario 1 (SC1). **b** Distance traveled under the raw speed profile and SC1. **c** Raw vehicle speed and adjusted speed under Scenario 2 (SC2). **d** Distance traveled under the raw speed profile and SC2. SC1 = Speed limit compliance without coasting. SC2 = Speed limit compliance with coasting.

source vehicle. This is also reflected in Fig. 7b, where the modified profile leads to a longer travel time over the same distance. On the other hand, when Scenario 2 is applied (see Fig. 7c), the virtual vehicle's speed is still capped at the posted speed limit, but it is allowed to coast down (decelerate) from when the deceleration begins to the closest local minimum speed at a rate that ensures it travels the required distance. In this case, the anchor point considered is the time step corresponding to this local minimum. Scenario 2 was introduced to avoid artificially enforcing positive tractive power during segments where the raw vehicle naturally decelerates from above the speed limit via near-zero-power coasting, a behavior that is suppressed under Scenario 1. Readers interested in the implementation details of the intervention scenarios can refer to the code in the GitHub repository, whose link is provided in the "Code availability" section.

Energy and cost savings estimation

To evaluate the energy consumption impacts of each intervention scenario, we simulate each trip using the calibrated energy consumption model matched to the trip's vehicle class and powertrain type, for the two considered interventions. We then resample the elevation profiles to match the time and distance profile of each modified speed profile, ensuring consistency with the original topography. We then feed the synchronized time, speed, and elevation profiles into the energy consumption model to simulate the trip. Each simulation computes second-by-second power demand, from which we derive energy consumption for each trip. For ICEVs, energy consumption is expressed in gallons of fuel, whereas for BEVs, it is expressed in kilowatt-hours (kWh). To estimate the energy savings as a percentage, we calculate the difference between the energy consumption of the virtual vehicles in each of the two scenarios and that of the source vehicle. We then normalize the energy savings by distance traveled to obtain savings per 100 miles for each trip, and use the average of these values at the geohash level to generate the choropleth maps in Figs. 3a, b, and 4a, b. Spatial aggregation for the choropleth maps was performed using 3-character geohashes to ensure uniform spatial resolution and to address data privacy constraints associated with connected-vehicle data. This grid-based representation reduces sensitivity to heterogeneous administrative boundaries and mitigates issues related to the modifiable areal unit problem. Additionally, state-level aggregation does not rely on geohashes. Each trip is assigned to a state based on the state code of its first recorded location, which is provided directly in the raw dataset.

To extrapolate the trip-level percentage savings of ICEVs from our dataset into real-world energy and cost impacts, we first calculated a representative daily VMT profile for each state. Since a unified public dataset reporting state-level VMT disaggregated by powertrain does not exist to the best of our knowledge, we constructed this metric by combining multiple federal data sources. We first calculated the annual state-level LD VMT for 2021 by combining FHWA Highway Statistics Tables VM-2[40] and VM-4[41]. VM-2 provides total annual VMT by state, area type (rural/urban), and functional class (interstate, arterials, etc.). VM-4 provides the percentage distribution of VMT by vehicle type within similar categories. For each area type, the functional classes defined in VM-2 are (1) Interstate, (2) Other freeways and expressways, (3) Other principal arterial, (4) Minor arterial, (5) Major collector, (6) Minor collector, and (7) Local. On the other hand, the functional classes defined in VM-4 are (1) Interstate, (2) Other arterials and (3) Others. To reconcile these, we mapped VM-2 classes 2 through 4 (Other freeways, principal arterials, and Minor arterials) to the VM-4 "Other arterials" category, and VM-2 classes 5 through 7 (Collectors and Local roads) to the VM-4 "Other" category. LD VMT was then computed by multiplying the total VMT in each mapped group by the combined percentage of passenger cars and light trucks reported in VM-4. To derive the ICEV component, we assume that annual VMT across fuel types scales proportionally with vehicle registration counts across fuel types. This is an approximation necessitated by the absence of state-level VMT data disaggregated by powertrain or fuel type. We use the DOE AFDC 2021 vehicle registration counts[42] dataset to determine these registration shares. These counts are approximate values derived from Experian data, are rounded to the closest 100 vehicles, and reflect the total number of LD registered vehicles through the selected year based on VIN-decoding and are used as a proxy for the on-road LD vehicle fleet. We defined the ICEV fleet as the sum of all non-hybrid, non-plug-in combustion powertrains. This includes gasoline, diesel, ethanol/flex (E85), biodiesel, CNG, propane, hydrogen, and methanol. We then calculate the ICEV fleet share by dividing this sum by the total LDV registrations. While our energy consumption models in FASTSim use the gasoline gallon equivalent of 33.7 kWh for energy consumption computation and tuned efficiency maps based on fuel economy values of gasoline vehicles for all ICEV trips, we included these diverse fuel types in our VMT allocation to capture the full scope of ICEV-based activity and avoid understating the true size of the non-EV fleet. Across all states, the mean ICEV share of the fleet is 96.79% (SD = 1.23%), while the specific gasoline-only share is 84.66% (SD = 3.26%). Given that non-gasoline ICEVs represent a modest fraction of total ICEV counts, we consider this simplification a reasonable approximation for the aggregate ICEV fleet.

To account for seasonal fluctuations in travel, we disaggregated the annual state-level LD VMT (for ICEVs) into month-specific daily volumes using monthly split factors (μ_m) derived from the FHWA December 2021 Traffic Volume Trends[43]. These factors represent the fraction of annual travel occurring in each month and are assumed to apply uniformly across the LD segment. For each state and month, we calculated a scaling factor by dividing the estimated real-world daily LD VMT (for ICEVs) by the total distance of the sampled trips in our dataset for that specific state and month. This factor was applied to the aggregated trip-level fuel savings to determine the absolute gallons saved per day. The daily estimated ICEV fuel savings for state s during month m, denoted as $\Delta F_{s,m}$, is calculated as:

$$\Delta F_{s,m} = \left(\frac{\mathrm{VMT}^{\mathrm{ICEV}}_{s,m}}{\sum_i d_{i,s,m}}\right) \times \sum_i \delta f_{i,s,m} \tag{2}$$

where $\sum d_{i,s,m}$ is the total distance traveled by all sampled trips i in our dataset for state s and month m, and $\sum \delta f_{i,s,m}$ is the corresponding aggregate fuel savings. The daily VMT (for ICEVs) ($\mathrm{VMT}^{\mathrm{ICEV}}_{s,m}$) is determined by:

$$\mathrm{VMT}^{\mathrm{ICEV}}_{s,m} = (\mathrm{VMT}^{\mathrm{LD}}_{s} \times \Phi^{\mathrm{ICEV}}_{s}) \times \frac{\mu_m}{N_m} \tag{3}$$

In this expression, $\mathrm{VMT}^{\mathrm{LD}}_{s}$ represents the annual LD VMT from the VM-2/VM-4 mapping, Φ^{ICEV}_{s} is the ICEV registration share, μ_m is the monthly VMT fraction, and N_m is the number of days in the given month.

For BEVs, we adopt a different scaling approach by utilizing direct electricity consumption data, which provides a more accurate representation of real-world energy consumption than VMT-based scaling. We retrieved the monthly national electricity consumption by LD BEVs and the state-wise annual consumption for 2021 from the EIA Electric Power Monthly[7]. We calculated California's share of national consumption using the annual state-wise data and assumed this proportion remained constant throughout the year. Applying this share to the national monthly data yielded monthly electricity consumption estimates for California, which we converted to daily averages by dividing by the number of days in each month. We then scaled the state-wide energy savings based on these daily averages to obtain absolute daily energy savings, which are plotted in Fig. 4e.

To estimate the cost savings under each intervention scenario, we use region- and day-specific gasoline (for ICEVs) and electricity (for BEVs) prices. For ICEVs, we use the average retail price of regular gasoline in each state on the date of the vehicle trips, based on data from ref. 44, which may introduce a slight bias for the small subset of non-gasoline ICEVs as discussed previously. For jurisdictions where direct state-level reporting was unavailable from ref. 44 ($n = 41$), prices were estimated using the corresponding sub-PADD (e.g., New England, Central Atlantic, and Lower Atlantic) or PADD regional averages (available from ref. 44). While this introduces a degree of spatial smoothing for those jurisdictions, these regional values provide the highest resolution retail gasoline price data available from federal sources for the study period. For BEVs, we use the average monthly residential electricity price in each state during the month of the vehicle trips, as over 82% of BEV charging occurs at home[45]. Electricity price data were obtained from ref. 46.

Carbon dioxide emissions reduction estimation

To estimate the potential reduction in CO_2 emissions, we use two rate values: (1) the carbon dioxide emissions coefficient (CEC) for ICEVs and (2) the marginal operating emissions rate (MOER) for BEVs. CEC is defined as the amount of CO_2 in kilograms emitted per gallon of gasoline consumed. In this study, we use the CEC of finished motor gasoline: 8.49 kg CO_2 per gallon[47]. This value assumes that all the carbon in gasoline is converted to CO_2. To estimate emissions savings, the fuel savings for each ICEV trip are multiplied by the CEC of finished motor gasoline. Equation 4 quantifies the CO_2 emissions in grams associated with V_{fuel} gallons of gasoline.

$$\mathrm{CO}_{2,\mathrm{ICEV}} = V_{\mathrm{fuel}} \times (8490\,\mathrm{g\,CO_2\,gal^{-1}}) \tag{4}$$

For BEVs, emissions depend on the grid's energy mix at the time of charging. The MOER, typically expressed in lbs MWh^{-1}, represents the emissions rate of the electricity generators responding to changes in load on the local grid at a particular time[48]. This is different from the average grid emissions rate, which represents the CO_2 intensity (i.e., emissions per unit of electricity generated) across all power plants in a region. The MOER estimates the CO_2 intensity of the next MWh of load added (or removed) from the grid at a given time. It accounts only for marginal generators, which are often fast-ramping, fossil-fueled plants and thus tend to have higher emission rates. We use MOER data calculated by WattTime[49], based on a proprietary model that extends the basic methodology used by both Siler-Evans et al.[50] and Callaway et al.[48] but adapted for real-time use. We use data for the California Independent System Operator (CAISO) across the 4 days in 2021, at a 5-min resolution. However, the dataset used in this study does not directly observe when charging occurs for the BEV trips. Therefore, we allocate the total per-day BEV energy savings across the 24 h of the day using an empirically derived diurnal distribution of residential BEV charging. This distribution is derived from the National Laboratory of the Rockies' Electric Vehicle Infrastructure Projection Tool (EVI-Pro), which simulates temporally resolved charging demand for California BEVs and PHEVs[22]. This model generates representative residential charging load profiles based on assumptions about vehicle travel behavior, home charging access, and charging start times. We parameterize the model to reflect LD BEVs with universal access to home charging using either of Level 1 or Level 2 chargers, and we generate weekday charging profiles for seasonal temperature conditions. The charging load profiles differ modestly across the 4 days due to differences in ambient temperature assumptions. The resulting load profiles are normalized and used solely to represent the temporal distribution of residential BEV charging within a day, independent of total daily electricity consumption. The MOER profiles and the normalized charging load distributions used in this analysis for each of the four days are illustrated in Supplementary Fig. 2a, b, respectively.

To estimate emissions savings, total daily BEV energy savings associated with the interventions are distributed across the 24 h of the day using the diurnal charging profile. Hourly average MOER values are then applied to the allocated energy to compute marginal CO_2 emissions, and daily emissions savings are obtained by summing across all hours. This approach links aggregate BEV energy savings to temporally resolved grid emissions conditions while remaining agnostic to the exact timing of individual charging events. Equation 5 quantifies the CO_2 emissions in grams associated with $E(d)$ of electric energy charged during day d, and $w(d, h)$ represents the fraction of daily charging load that occurs on hour h of day d. Here, the $\mathrm{MOER}_{d,h}$ represents the MOER averaged over that specific hour and day.

$$\mathrm{CO}_{2,\mathrm{BEV}}(d) = \sum_{h=0}^{23}\left[E(d) \times w(d,h) \times \mathrm{MOER}(d,h) \times (453.592\,\mathrm{g\,lb^{-1}}) \times \frac{1}{1000}\right] \tag{5}$$

Because the charging schedule (when and for how long BEVs are charged) relative to trip activity is not directly observed and may vary across drivers, we perform a sensitivity analysis considering multiple charging schedule specifications. These alternative modeling assumptions are described below and are used to assess the sensitivity of emissions outcomes to plausible charging behaviors.

Daily weighted: as described above, this scenario uses a weighted average MOER across all 24 h with weights from the empirical load distribution. This assumes that all BEV charging occurs using residential chargers (L1 or L2) and follows the considered load distribution.

Overnight weighted: this scenario uses the same load distribution to calculate the weights but restricts charging to residential overnight hours (22:00 to 06:00). This scenario addresses the observation that most at-home charging occurs overnight[51] while preserving the nonuniform within-overnight distribution (e.g., higher charging rates at 22:00 to 23:00 and midnight compared to 03:00 to 05:00). This scenario tests whether focusing exclusively on residential overnight charging meaningfully changes emissions estimates.

Overnight unweighted: this scenario assumes charging is evenly distributed across overnight hours (22:00 to 06:00) with equal probability in each hour. This removes empirical weighting and represents a simplified overnight-only charging assumption.

Daily unweighted: this scenario assumes charging is equally likely during all hours of the day. This represents an extreme case of fully unconstrained charging behavior with no temporal preferences, and provides a comparison baseline for assessing the value of empirical weighting.

Best hour (minimum MOER): this scenario assigns all BEV charging to the hour with the minimum average MOER on each study day. It represents an idealized lower bound on charging-related emissions and is not intended to reflect feasible driver behavior or charging logistics. Rather, it serves as a theoretical benchmark against which more realistic charging scenarios can be compared.

Worst hour (maximum MOER): this scenario assigns all BEV charging to the hour with the maximum average MOER on each study day. It represents an idealized upper bound on charging-related emissions and serves as a counterfactual benchmark for evaluating the range of possible emissions outcomes under alternative charging assumptions.

For the daily and overnight charging scenarios, MOER values are drawn exclusively from the 24 h of the same calendar day, rather than including late-night hours from the preceding day. In practice, overnight charging for early-morning trips may begin on the previous evening (e.g., the night of January 5 for trips occurring on January 6). We adopt this simplification to avoid introducing additional assumptions regarding the exact charging start time on the preceding day. This approach implicitly assumes that intraday MOER patterns are similar across consecutive days, such that excluding late-night hours from the prior day does not materially affect emissions estimates.

Extrapolation assumptions

For the extrapolated ICEV fleet, aggregate daily energy, cost, and emissions impacts are obtained by scaling state-aggregated fuel savings from the observed ICEV fleet using state-wise, real-world average daily VMT for each month. A limitation of this VMT-normalized extrapolation is that it does not explicitly distinguish between weekday and weekend driving behavior. The 2022 American Driving Survey[52] reported that average daily miles driven on Wednesdays are lower than the weekly mean and substantially lower than peak travel days, such as Thursdays and Fridays. Because the four analyzed days correspond to Wednesdays, this scaling results in an overestimation of total daily savings for those specific Wednesdays. Conversely, when interpreted as representative average daily impacts, this approach may underestimate savings on higher-VMT days, such as Thursdays and Fridays, which contribute disproportionately to monthly VMT. Congestion levels and speeding prevalence between different days of the week may further influence per-mile energy, cost, and emissions impacts. Two of the analyzed days also fall within the COVID-19 recovery period in early 2021, when national VMT remained below historical norms[43]. While this does not affect the trip-level speeding and energy impacts quantified here, it may influence the representativeness of the VMT-scaled extrapolation for non-pandemic travel conditions. Accordingly, the reported values should be interpreted as VMT-scaled estimates of average daily savings, rather than precise reconstructions of day-specific travel behavior.

In this study, the extrapolation of energy, emissions, and cost savings differs between ICEVs and BEVs. In principle, scaling based on direct energy consumption is preferable, as it avoids the implicit assumption that all vehicles accrue similar annual mileage regardless of powertrain or fuel type. However, for ICEVs, the absence of state-level, LD fuel consumption data necessitates a VMT-based extrapolation. Aggregate gasoline sales data are poorly suited for this purpose because they include substantial non-transport uses and fuel consumption from vehicle classes outside the scope of this analysis, preventing the isolation of LD ICEV travel. In contrast, for BEVs, the availability of state-wise electricity consumption estimates for LD BEV charging enables a consumption-based scaling that more directly reflects real-world vehicle energy use. This asymmetry in data availability leads to different extrapolation strategies, which further limit strict quantitative comparability between ICEV and BEV national totals. The extrapolated values should be interpreted as indicative of system-level impacts of reduced speeding behavior within each powertrain class, rather than as precise cross-powertrain forecasts, with relative trends and seasonal patterns remaining robust.

Emissions modeling assumptions

The ICEV emissions savings estimates reported in this study are based on combustion (tank-to-wheel) emission factors. This excludes upstream emissions associated with crude oil recovery, transport, and refining. Using CA-GREET 3.0, upstream fuel production and distribution processes account for approximately 27% of total well-to-wheel emissions for California reformulated gasoline (CARBOB)[53]. Accounting for these upstream contributions would increase the absolute ICEV GHG savings by approximately 37% relative to the combustion-only estimates. This adjustment scales proportionally with fuel consumption and does not affect the seasonal trends of the ICEV fleet reported here. However, incorporating upstream emissions does impact the relative comparison between the ICEV and BEV fleets. Because emissions of the BEV fleet are calculated using MOER, the BEV boundary is effectively well-to-wheel for the operational phase of the vehicles, as they account for grid-side emissions. Conversely, this study adopts the tank-to-wheel boundary for the ICEV fleet to provide a conservative, observation-based lower bound of driver-behavior impacts that remains independent of the specific efficiencies of the gasoline supply chain. The tank-to-wheel ICEV boundary, therefore, understates the operational use-phase emissions-reduction potential of the ICEV fleet relative to the BEV fleet. However, we acknowledge that this creates a boundary mismatch in the comparison. We also emphasize that these results characterize use-phase impacts only, and a full cradle-to-grave assessment, which includes the emissions-intensive manufacturing of vehicles and batteries, would be required to determine the absolute life-cycle benefit of either fleet.

Data availability

The primary dataset used in this study is proprietary and cannot be shared publicly due to privacy restrictions. Researchers interested in accessing the data for collaborative purposes may contact the corresponding author to explore potential data-sharing agreements. Source data for the figures in the main text are publicly available in the referenced Figshare repository[54].

Code availability

All the code, including the energy consumption models, used to generate the results presented in this study, is publicly available at: https://github.com/bharatwrrr/cost-of-speed.

Received: 10 November 2025; Accepted: 28 May 2026;
Published online: 16 July 2026

References

1. U.S. Energy Information Administration. International Energy Outlook 2023, accessed 26 June 2025, https://www.eia.gov/outlooks/ieo/ (2023).
2. International Energy Agency. World Energy Mix, accessed 26 June 2025, https://www.iea.org/world/energy-mix (2025).
3. U.S. Energy Information Administration. Monthly Energy Review, 2024 editions, accessed 27 June 2025, https://www.eia.gov/totalenergy/data/monthly/ (2024).
4. U.S. Energy Information Administration. Gasoline and Diesel Fuel Update, accessed 27 June 2025, https://www.eia.gov/petroleum/gasdiesel/ (2025).
5. Alliance for Automotive Innovation. *Get Connected Electric Vehicle Quarterly Report, Second Quarter 2025*. Technical report, accessed 30 October 2025, https://www.autosinnovate.org/posts/papers-reports/Get%20Connected%20EV%20Quarterly%20Report%20202%20Q2.pdf (Alliance for Automotive Innovation, 2025).
6. Argonne National Laboratory. Light-Duty Electric Drive Vehicles Monthly Sales Updates, accessed 4 February 2026, https://www.anl.gov/esia/light-duty-electric-drive-vehicles-monthly-sales-updates (2025).
7. U.S. Energy Information Administration. Electric Power Monthly, accessed 27 June 2025, https://www.eia.gov/electricity/monthly/ (2024).
8. U.S. Energy Information Administration. *EIA-861m Monthly Electric Power Industry Report*, accessed 27 June 2025 (U.S. Energy Information Administration EIA, 2024).
9. U.S. Environmental Protection Agency. Greenhouse Gas Equivalencies Calculator: Calculations and References, accessed 17 July 2025, https://www.epa.gov/energy/greenhouse-gas-equivalencies-calculator-calculations-and-references (2025).
10. Hucho, W.-H. *Aerodynamics of Road Vehicles: from Fluid Mechanics to Vehicle Engineering* (Elsevier, 2013).
11. Barth, M. & Boriboonsomsin, K. Real-world carbon dioxide impacts of traffic congestion. *Transp. Res. Rec.* **2058**, 163–171 (2008).
12. Blomquist, G. The 55 m.p.h speed limit and gasoline consumption. *Resour. Energy* **6**, 21–39 (1984).
13. Gao, C., Xu, J., Jia, M. & Sun, Z. Correlation between carbon emissions, fuel consumption of vehicles and speed limit on expressway. *J. Traffic Transp. Eng.* **11**, 631–642 (2024).
14. Fondzenyuy, S. K. et al. The impact of speed limit change on emissions: a systematic review of literature. *Sustainability* **16**, 7712 (2024).
15. Thomas, J., Huff, S., West, B. & Chambon, P. Fuel consumption sensitivity of conventional and hybrid electric light-duty gasoline vehicles to driving style. *SAE Int. J. Fuels Lubr.* **10**, 672–689 (2017).
16. Galvin, R. Energy consumption effects of speed and acceleration in electric vehicles: laboratory case studies and implications for drivers and policymakers. *Transp. Res. Part D Transp. Environ.* **53**, 234–248 (2017).
17. Barla, P., Gilbert-Gonthier, M., Castro, M. A. L. & Miranda-Moreno, L. Eco-driving training and fuel consumption: impact, heterogeneity and sustainability. *Energy Econ.* **62**, 187–194 (2017).
18. Dahlinger, A. et al. The impact of numerical vs. symbolic eco-driving feedback on fuel consumption–a randomized control field trial. *Transp. Res. Part D Transp. Environ.* **65**, 375–386 (2018).
19. Richard, C. M., Lee, J., Atkins, R. & Brown, J. L. Using SHRP2 naturalistic driving data to examine driver speeding behavior. *J. Saf. Res.* **73**, 271–281 (2020).
20. National Highway Traffic Safety Administration. *Continuation of Research on Traffic Safety during the COVID-19 Public Health Emergency: January-June 2021*. Technical report, https://doi.org/10.21949/1526036 (U.S. Department of Transportation, National Highway Traffic Safety Administration, 2021).
21. Brooker, A. et al. *FASTSim: A Model to Estimate Vehicle Efficiency, Cost and Performance*. Technical report, SAE Technical paper (SAE International, 2015).
22. Lee, D.-Y., Reinicke, N., Wood, E., Ge, Y. & Burrell, E. *Electric Vehicle Infrastructure Projection Tool (EVI-Pro)*. Technical report (National Renewable Energy Laboratory, 2021).
23. Administration, U.S.F.H. *Table VM-1: Annual Vehicle Distance Traveled in Miles and Related Data*. Technical report, https://www.fhwa.dot.gov/policyinformation/statistics/2021/pdf/vm1.pdf (U.S. Department of Transportation, Federal Highway Administration, 2021).
24. Administration, U.S.E.I. *2020 Residential Energy Consumption Survey: Detailed End-Use Consumption and Expenditure Estimates*, Technical report, https://www.eia.gov/consumption/residential/data/2020/index.php?view=consumption (U.S. Department of Energy, Energy Information Administration, 2023).
25. Gelman, M. et al. The response of consumer spending to changes in gasoline prices. *Am. Econ. J. Macroecon.* **15**, 129–160 (2023).
26. Baumeister, C. & Kilian, L. Lower oil prices and the US economy: is this time different? *Brook. Pap. Econ. Act.* **2016**, 287–357 (2016).
27. U.S. Energy Information Administration. How much tax do we pay on a gallon of gasoline and on a gallon of diesel fuel? Accessed 29 July 2025, https://www.eia.gov/tools/faqs/faq.php?id=10&t=5 (2024).
28. Interagency Working Group on Social Cost of Greenhouse Gases. *Technical Support Document: Social Cost of Carbon, Methane, and Nitrous Oxide: Interim Estimates under Executive Order 13990*. Technical report, accessed 29 July 2025, https://www.energy.gov/sites/default/files/2023-04/57.%20Social%20Cost%20of%20Carbon%202021.pdf (Interagency Working Group on Social Cost of Greenhouse Gases, United States Government 2021).
29. Peer, E. The time-saving bias, speed choices and driving behavior. *Transp. Res. Part F Traffic Psychol. Behav.* **14**, 543–554 (2011).
30. Bricka, S. et al. *Summary of Travel Trends: 2022 National Household Travel Survey*. Technical report (Federal Highway Administration, Office of Policy and Governmental Affairs, 2024).
31. Ellison, A. B. & Greaves, S. P. Speeding in urban environments: are the time savings worth the risk? *Accid. Anal. Prev.* **85**, 239–247 (2015).
32. Zhao, L., Ottinger, E. R., Yip, A. H. C. & Helveston, J. P. Quantifying electric vehicle mileage in the United States. *Joule* **7**, 2537–2551 (2023).
33. National Highway Traffic Safety Administration. *Speeding: 2023 Data*. Technical report No. DOT HS 813 721, https://crashstats.nhtsa.dot.gov/Api/Public/ViewPublication/813721 (U.S. Department of Transportation, National Highway Traffic Safety Administration, 2025).
34. OpenStreetMap contributors. Planet dump retrieved from, https://www.openstreetmap.org (2017).
35. Insurance Institute for Highway Safety. Maximum Posted Speed Limits, https://www.iihs.org/research-areas/speed/speed-limit-laws (2025).
36. U.S. Geological Survey. 3D Elevation Program 1/3 Arc-Second Digital Elevation Model, accessed 30 June 2025, https://www.usgs.gov/the-national-map-data-delivery (2020).
37. U.S. Environmental Protection Agency. Data on Cars Used for Testing Fuel Economy, accessed 4 March 2025, https://www.epa.gov/compliance-and-fuel-economy-data/data-cars-used-testing-fuel-economy (2025).
38. Mindell, J. S., Leslie, D. & Wardlaw, M. Exposure-based, ‘like-for-like’ assessment of road safety by travel mode using routine health data. *PLoS ONE* **7**, e50606 (2012).
39. Gao, F. & Han, L. Implementing the Nelder-Mead simplex algorithm with adaptive parameters. *Comput. Optim. Appl.* **51**, 259–277 (2012).

40. U.S. Department of Transportation, Federal Highway Administration. *Table vm-2: Highway Statistics 2021*, accessed 29 January 2026, https://www.fhwa.dot.gov/policyinformation/statistics/2021/vm2.cfm (2023).
41. Federal Highway Administration. Table vm-4: Distribution of Annual Vehicle Distance Traveled 2021, accessed 3 February 2026, https://www.fhwa.dot.gov/policyinformation/statistics/2021/vm4.cfm (2023).
42. U.S. Department of Energy, Alternative Fuels Data Center. *Vehicle Registration Counts by State: 2021*, accessed 29 January 2026, https://afdc.energy.gov/vehicle-registration?year=2021 (2022).
43. Federal Highway Administration, U.S. Department of Transportation. *Traffic Volume Trends—December 2021*, accessed 3 February 2026, https://www.fhwa.dot.gov/policyinformation/travel_monitoring/21dectvt/ (2021).
44. U.S. Energy Information Administration. EIA Open Data: Monthly Gasoline And Diesel Retail Prices, accessed 27 June 2025, https://www.eia.gov/opendata/browser/petroleum/pri/gnd?frequency=monthly&data=value;&start=2021-01&end=2025-05&sortColumn=period;&sortDirection=desc (2025).
45. Hurlbut, D. J., McLaren, J. A., Koebrich, S., Williams, J. & Chen, E. I. *Electric Vehicle Charging Implications for Utility Ratemaking in Colorado*. Technical report (National Renewable Energy Laboratory, 2019).
46. U.S. Energy Information Administration. EIA Open Data: Monthly Electricity Retail Prices by Sector, accessed 27 June 2025, https://www.eia.gov/opendata/browser/electricity/retail-sales?frequency=monthly&data=price;&facets=sectorid;&sectorid=ALL;COM;RES;&start=2024-01&end=2025-03&sortColumn=period;&sortDirection=desc; (2025).
47. U.S. Energy Information Administration. Carbon Dioxide Emissions Coefficients, accessed 9 July 2025, https://www.eia.gov/environment/emissions/co2_vol_mass.php (2024).
48. Callaway, D. S., Fowlie, M. & McCormick, G. Location, location, location: the variable value of renewable energy and demand-side efficiency resources. *J. Assoc. Environ. Resour. Econ.* **5**, 39–75 (2018).
49. WattTime API. CO_2 Marginal Operating Emissions Rate, accessed 31 August 2024, Data set, retrieved from https://api.watttime.org (2024).
50. Siler-Evans, K., Azevedo, I. L. & Morgan, M. G. Marginal emissions factors for the US electricity system. *Environ. Sci. Technol.* **46**, 4742–4748 (2012).
51. Kim, J. D. Insights into residential EV charging behavior using energy meter data. *Energy Policy* **129**, 610–618 (2019).
52. Steinbach, R. & Tefft, B. C. *American Driving Survey: 2022*. Research Brief (AAA Foundation for Traffic Safety, 2023).
53. California Air Resources Board. *CA-GREET3.0 Lookup Table Pathways: Technical Support Documentation*. Technical report, accessed 3 February 2026, https://ww2.arb.ca.gov/sites/default/files/classic/fuels/lcfs/ca-greet/lut-doc.pdf (California Air Resources Board, 2018).
54. Jayaprakash, B. Data for: speeding incurs substantial environmental and economic costs for negligible travel time savings nationwide, https://doi.org/10.6084/m9.figshare.32226726.v1 (2026).

Acknowledgements
Map data copyrighted OpenStreetMap contributors and available from https://www.openstreetmap.org. This material is based upon work partially supported by the National Science Foundation under grant no. 1901099.

Author contributions
Bharat Jayaprakash led the research design, performed the large-scale vehicle trajectory analysis, developed the emissions and energy modeling framework, interpreted the results, and drafted the original manuscript. William Northrop secured the funding and purchased the dataset used for the analysis, supervised the study, provided critical feedback on the methodology and findings, and contributed to the writing and editing of the manuscript. Both authors reviewed and approved the final version of the manuscript.

Competing interests
The authors declare no competing interests.

Additional information
Supplementary information The online version contains Supplementary material available at https://doi.org/10.1038/s44458-026-00100-3.

Correspondence and requests for materials should be addressed to Bharat Jayaprakash or William F. Northrop.

Peer review information *Communications Sustainability* thanks Matthew Bruchon and the other anonymous reviewer(s) for their contribution to the peer review of this work. Primary handling editors: Zhao Xu and Nandita Basu. A peer review file is available.

Reprints and permissions information is available at http://www.nature.com/reprints

Publisher's note Springer Nature remains neutral with regard to jurisdictional claims in published maps and institutional affiliations.